



Multiple Coulomb scattering method to reconstruct low-energy gamma-ray direction in the GAMMA-400 space-based gamma-ray telescope

A.A. Leonov^{a,b,*}, A.M. Galper^{a,b}, N.P. Topchiev^a, A.V. Bakaldin^{a,c}, O.D. Dalkarov^a
E.A. Dzhivelikyan^b, A.E. Egorov^a, M.D. Kheyimits^b, V.V. Mikhailov^b, P. Picozza^{d,e}
R. Sparvoli^{d,e}, S.I. Suchkov^a, Yu.T. Yurkin^b, V.G. Zverev^a

^a *Lebedev Physical Institute, Russian Academy of Sciences, Moscow 119991, Russia*

^b *National Research Nuclear University MEPhI, Moscow 115409, Russia*

^c *Scientific Research Institute for System Analysis, 117218 Moscow, Russia*

^d *Istituto Nazionale di Fisica Nucleare, Sezione di Roma 2, Rome, Italy*

^e *Physics Department of University of Rome Tor Vergata, Rome, Italy*

Received 9 November 2018; received in revised form 16 January 2019; accepted 24 January 2019

Available online 1 February 2019

Abstract

The GAMMA-400 currently developing space-based gamma-ray telescope is designed to measure the gamma-ray fluxes in the energy range from ~ 20 MeV to several TeV in the highly elliptic orbit (without shadowing the telescope by the Earth) continuously for a long time. The physical characteristics of the GAMMA-400 gamma-ray telescope, especially the angular and energy resolutions (at 100-GeV gamma rays they are $\sim 0.01^\circ$ and $\sim 1\%$, respectively), allow us to consider this space-based experiment as the next step in the development of extraterrestrial high-energy gamma-ray astronomy. In this paper, a method to improve the reconstruction accuracy of incident angle for low-energy gamma rays in the GAMMA-400 space-based gamma-ray telescope is presented. The special analysis of topology of pair-conversion events in thin layers of converter was performed. Applying the energy dependence of multiple Coulomb scattering for pair components, it is possible to estimate the energies for each particle, and to use these energies as weight in the angle reconstruction procedure. To identify the unique track in each projection the imaginary curvature method is applied. It allows us to obtain significantly better angular resolution in comparison with other methods applied in current space-based experiments. When using this method for 50-MeV gamma rays the GAMMA-400 gamma-ray telescope angular resolution is about 4° .

© 2019 COSPAR. Published by Elsevier Ltd. All rights reserved.

Keywords: Gamma-ray; Converter-tracker; Angular resolution; GEANT4 simulation toolkit; Coulomb scattering

1. Introduction

The GAMMA-400 instrument was developed to solve a broad range of scientific goals, such as sensitive searching for high-energy gamma-ray emission when annihilating

or decaying dark matter particles and searching for new and studying known Galactic and extragalactic discrete high-energy gamma-ray sources (supernova remnants, pulsars, accreting objects, microquasars, active galactic nuclei, blazars, quasars, etc.) (Topchiev et al., 2016a, 2016b). The major advantage of the GAMMA-400 instrument is excellent angular and energy resolutions for gamma rays above 10 GeV. The gamma-ray telescope angular and energy

* Corresponding author.

E-mail address: leon@ibrae.ac.ru (A.A. Leonov).

resolutions for the main aperture at 100-GeV gamma rays are $\sim 0.01^\circ$ and $\sim 1\%$, respectively. Thus, it will be possible to study the structure of astrophysical objects with high angular resolution, measuring their energy spectra and luminosity with high-energy resolution and identifying discrete gamma-ray sources with known sources of electromagnetic emission in other energy ranges.

The motivation of presented results is to provide the methodical approaches improving physical characteristics of the GAMMA-400 gamma-ray telescope in the energy range of ~ 20 – 100 MeV, most unexplored range today (De Angelis et al., 2018). Gamma-ray observations in this energy range are crucial today for a number of high-priority problems faced by modern astrophysics and fundamental physics, including the origin of chemical elements and cosmic rays, the nature of dark matter, and the applicability range of the fundamental laws of physics.

The location of the high-energy gamma-ray sources in the Universe is determined through the reconstruction of the directions of gamma rays. In the GAMMA-400 gamma-ray telescope, this direction is measured via the conversion of gamma rays in thin tungsten foils in the converter-tracker and the subsequent reconstruction of the electron/positron pair with a precise silicon tracker. The energy measurement is provided by calorimeter. The converter introduces, however, an unavoidable error in the direction determination due to the multiple Coulomb scattering of the trajectory of particles. It is crucial to understand how the multiple scattering affects the reconstruction of angular resolution. The detector layers of the GAMMA-400 converter-tracker will provide the measurements of electron/positron tracks (with measurement errors). Depending on the energy of electrons, the effects of multiple scattering can be larger, the same, or smaller than the effects of measurement error. Large uncertainties in the arrival directions of gamma rays hamper the analysis of point sources at energies below 100 MeV. As a result, the confusion among point sources, difficulties in separating point sources from diffuse emission and high contamination from the Earth limb are arisen. The attempt to close a gap of point source analysis between the COMPTEL (<30 MeV) (Schonfelder et al., 2000) and the Fermi-LAT catalogs (>100 MeV) (Acero et al., 2015; Ackermann et al., 2013) was recently provided through the construction of first Fermi Large Area Telescope low-energy catalog (1FLE) (Principe et al., 2018). The accuracy of angle and energy reconstructions is insufficient, and special wavelet transform procedure was used to extract the point sources.

Usually, in the track reconstruction methods, like Kalman filter (Giuliani et al., 2006), multiple scattering is considered as a noise, which contaminates the main signal. In this paper, to determine incident gamma-ray direction in the telescope, we propose to use the energy dependence of multiple scattering for pair components induced by gamma-ray conversion with energy less than 100 MeV. Such approach is the further development of the procedure proposed previously in (Leonov et al., 2017). In this way,

we consider only three first planes of pair components in each projection that is enough to evaluate the energy weights for the electron/positron angles. These energy weights are further used to calculate incident gamma-ray direction. The calculation considers several approximations, such as the assumption of a Gaussian distribution of the multiple scattering (ignoring the important non-Gaussian tails) or neglecting the effects of the recoil of nucleus. There are other instrumental problems not considered here, like the pattern recognition, inefficiencies, and dead areas. However, this calculation provides a quantitative improvement of angular resolution at energies below 100 MeV.

2. The GAMMA-400 physical scheme

The GAMMA-400 physical scheme is shown in Fig. 1. GAMMA-400 consists of plastic scintillation top and lateral detectors (AC_{top} and AC_{lat}) forming anticoincidence system, a converter-tracker (C), plastic scintillation detectors (S1 and S2) for a time-of-flight system (ToF), a two-part calorimeter (CC1 and CC2), plastic scintillation detectors (S3 and S4) forming additional trigger.

The anticoincidence detectors surrounding the converter-tracker are used to distinguish gamma rays from significantly larger number of charged particles (in the energy range of 10–100 GeV, the flux ratios for gamma rays to electrons and protons are $\sim 1:10^2:10^5$ (Moiseev et al., 2007)).

All scintillation detectors consist of two independent layers, with thickness of 1 cm for each layer. The time-of-flight system, where detectors S1 and S2 are separated by approximately 500 mm, determines the top-down direction of arriving particles. The dimensions and location of detectors S1 and S2 determines gamma-ray telescope field of view (FoV), which is about $\pm 45^\circ$. The additional scintillation detectors S3 and S4 improve hadrons and electromagnetic showers separation.

The converter-tracker consists of 13 layers of double (x , y) silicon strip coordinate detectors (pitch of 0.08 mm). The first seven layers are interleaved with tungsten conversion foils with $0.1 X_0$ (where X_0 is the radiation length), next four layers are interleaved with tungsten conversion foils with $0.025 X_0$ and final two layers have no tungsten. Using the four $0.025 X_0$ layers allows us to measure gamma rays down to 20 MeV. In this case, the gamma-ray trigger for the energy range of 20–100 MeV and 100 MeV – 1000 GeV is the same: $\overline{AC} \times \text{ToF}$. The total converter-tracker thickness is $\sim 1 X_0$. The converter-tracker information is used to precisely determine the direction of each incident particle. The accuracy of the determination of incident particle direction is the goal for the studying in this paper.

The two-part calorimeter measures the particle energy. The CC1 imaging calorimeter consists of 2 layers of double (x , y) silicon strip coordinate detectors (pitch of 0.08 mm)

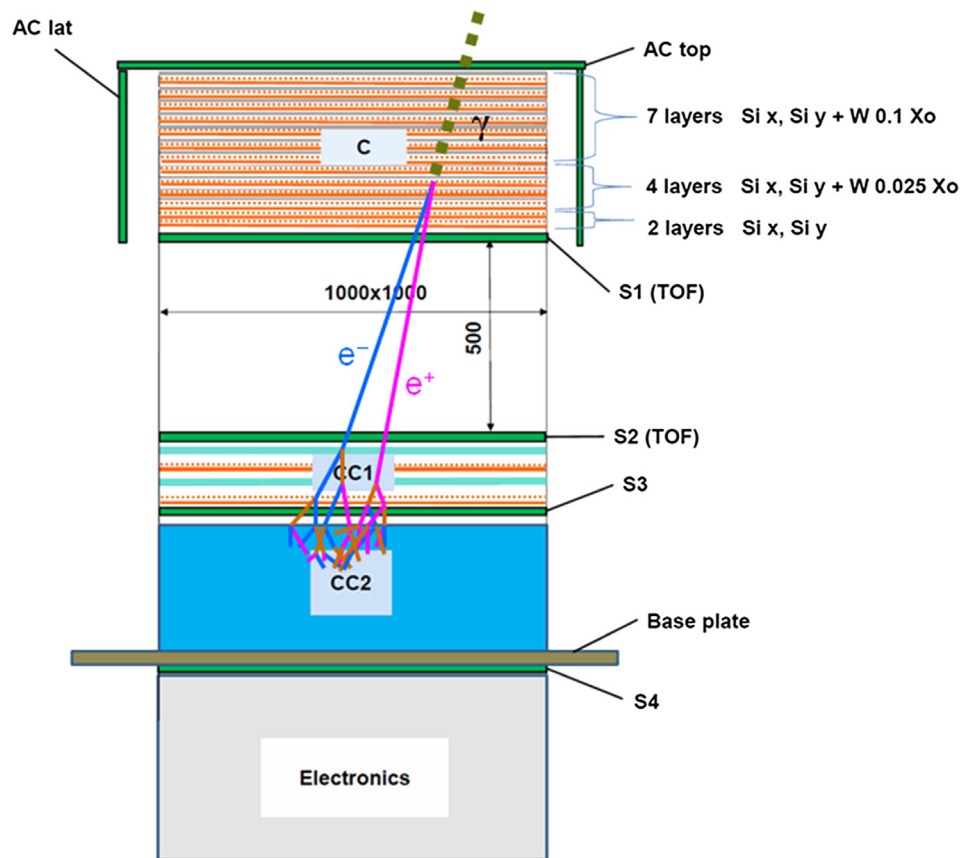


Fig. 1. The GAMMA-400 physical scheme.

interleaved with planes from CsI(Tl) crystals, and the CC2 electromagnetic calorimeter consists of CsI(Tl) crystals. The thickness of CC1 and CC2 is $2 X_0$ and $20 X_0$, respectively. The total calorimeter thickness is $\sim 22 X_0$ or $\sim 1 \lambda_0$ (where λ_0 is the nuclear interaction length). Using the deep calorimeter allows us to extend the energy range up to several TeV for gamma rays and ~ 10 TeV for electrons + positrons and to reach an energy resolution about $\sim 1\%$ at 100 GeV.

3. Simulation environment and data for the calculations

For simulating the passage of gamma rays through the GAMMA-400 matter, the GEANT4 toolkit (Allison et al., 2016) was used. Angular resolution was calculated for vertical gamma rays with energies from 10 to 150 MeV, which were converted into the electron/positron pair at first or any following tungsten conversion foil with $0.025 X_0$. For such events the information about the strip numbers with signal from energy release of charged particles and the values of energy release are retained. Gamma rays can also convert in the rest of the converter-tracker tray containing support matter, but these events are not considered here. The detailed description of material composition of this tray and the methodology to identify the tungsten conversion events are presented in (Leonov et al., 2017).

To calculate the energy dependence of multiple Coulomb scattering for pair components vertical and declined (30°) electrons with different energies were also generated.

4. Reconstruction of low-energy gamma-ray direction

Electron/positron passing through the converter-tracker matter suffers multiple elastic Coulomb scattering on nuclei. Since mass of nuclei is greater than incoming electron/positron, the energy transfer is negligible, but each scattering center adds a small deviation to the incoming particle trajectory. Even if this deviation is small the sum of all contributions adds a random component to the particle track. As a result, the initial direction of incoming electron/positron is changed. When the thickness of matter increases and the number of interactions becomes high, the angular dispersion can be modelled as Gaussian.

When the energy of the incident gamma rays is less than 150 MeV, each component of e^+/e^- pair produced after conversion in tungsten layer can be readily tracked individually.

The information from double (x, y) silicon strip coordinate detectors provides the possibility to split the total space development of conversion event in two perpendicular plane projections. Each projection, called as X or Y , is considered independently.

For the next analysis, gamma rays converted in thin (0.025 X_0) tungsten layers are only considered. In the converter-trackers, even if there is only one hit, due to capacitive coupling between adjacent strips, multiple strip segments are fired. But, taking into account the possibility of analog readout, the evaluation of the cluster position by means of the center of gravity method allows us to improve significantly the spatial resolution of strip sample and tracking accuracy (Berra et al., 2015). In the following for the sake of simplicity the tracks, consisting from single points (calculated as center of cluster position, if necessary) are considered.

For each event, presented by two tracks of e^+/e^- pair, the information about hit strips in first three X planes and in first three Y planes is used. The left strips with hits in each projection make “left” track (for electron, as example) and the right strips with hits make “right” track (for positron, as example). It is necessary to mention that strictly speaking, the two tracks cannot be surely identified, as pair components can cross and alter their relative position to the opposite one from one layer to another, but with low probability in the GAMMA-400 converter-tracker (Kheymits et al., 2015).

Fig. 2 shows red and purple piecewise lines for electron and positron tracks, respectively. Thus, each track contains six points: three points in the X projection and three points in the Y projection. The first point in the X projection, which is closest to the conversion point in tungsten, is common for both tracks ($x_0^- = x_0^+$). In this interpretation, one delicate point is arisen. How is it possible to determine the correspondence between the “left” and “right” tracks in different projections?

To resolve the problem the following procedure is applied.

For given projection each track of electron or positron due to multiple Coulomb scattering can be represented as three points in successive layers of converter-tracker,

through which a circle can be uniquely drawn with the imaginary curvature radius. In this way, for the X projection in left part of Fig. 2, there are two values: R_x^L and R_x^R , corresponding to the “left” X electron track and the “right” X positron track, respectively. In the same manner, the values R_y^L and R_y^R for the Y projection correspond to the “left” Y positron and “right” Y electron tracks, respectively. The reasonable assumption is that the track of more energetic particle has higher imaginary curvature radius in both projections. For the case, shown in Fig. 2 ($R_x^L > R_x^R$, $R_y^L < R_y^R$), the left track in the projection X and the right track in the projection Y belong to the electron track, while the right track in the projection X and the left track in the projection Y belong to the positron track.

Using the value of strip size and the value of vertical distance between the planes with silicon strip coordinate detectors it is straight forward to calculate plane angles with vertical for e^+/e^- pair: α_x^-, α_x^+ and α_y^-, α_y^+ (Fig. 3). From these plane angles for e^+/e^- pair and using the conservation of initial gamma-ray transverse momentum through relativistic e^+/e^- components the plane angles of initial gamma are derived as following:

$$\alpha_x = \frac{\alpha_x^- \times E^- + \alpha_x^+ \times E^+}{E^- + E^+} \tag{1}$$

$$\alpha_y = \frac{\alpha_y^- \times E^- + \alpha_y^+ \times E^+}{E^- + E^+}, \tag{2}$$

where E^-, E^+ are the energies of electron and positron, respectively.

Unlike the previous approach (Leonov et al., 2017), in which the energies of electron and positron were calculated for each projection independently using the dependence of imaginary curvature radius from energy, here, we determine the energies of electron and positron using the direct dependence of multiple Coulomb scattering from the energy, as $\sim 1/E$.

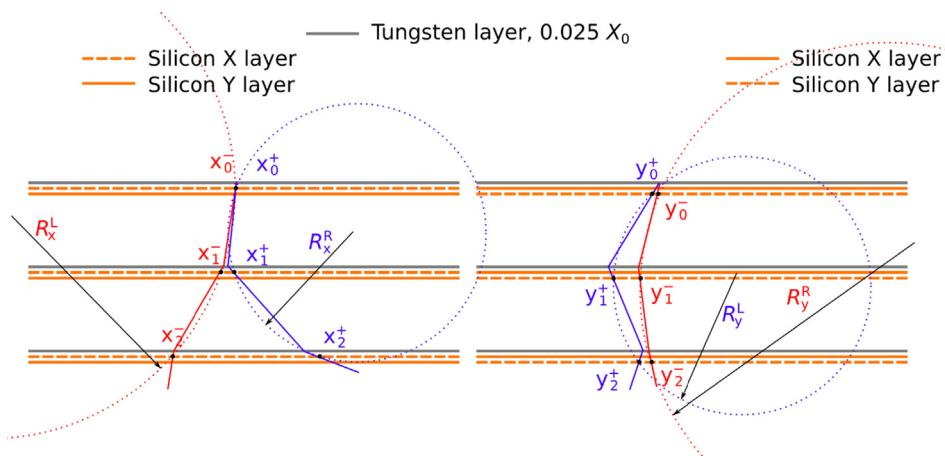


Fig. 2. Two tracks of e^+/e^- pair in X (left) and Y (right) projections. Gray lines are tungsten layers with thickness 0.025 X_0 . Orange lines are double (x, y) silicon strip coordinate detectors. (For interpretation of the references to colour in this figure legend, the reader is referred to the web version of this article.)

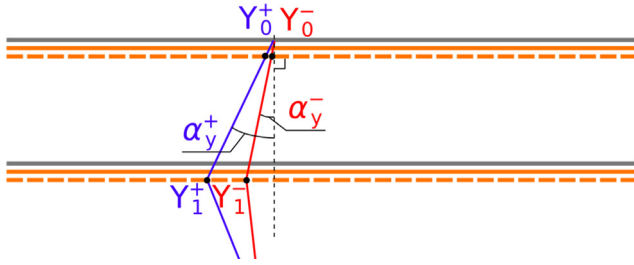


Fig. 3. Plane angles with vertical for e^+/e^- pair in the Y projection.

To obtain the dependence of multiple Coulomb scattering from energy of electron/positron in the GAMMA-400 converter-tracker the simulation of electron beam along vertical direction at first thin tungsten foil ($0.025 X_0$) was performed for energy range from 10 to 500 MeV. Two plane angles of electron trajectory were determined and retained for the X projection and also for the Y projection. The number of plane angles (two in the X projection and two in the Y projection) is an optimal value due to the track length of low energy particles in converter-tracker and in view of the generation of multiple tracks in several converter layers.

Fig. 4 shows an example of electron trajectory in the GAMMA-400 converter-tracker, which is marked by blue line. Three scattering points in tungsten layers are shown by black points. Magenta broken line corresponds to the trajectory restored using information from silicon strip detectors due to the converter-tracker granularity.

Plane angle $\alpha_{x1}^{strip} = \alpha_{x1}$ is the estimation of the electron trajectory deviation after the multiple Coulomb scattering in first and second tungsten layers. It is calculated using the information from first and second planes of silicon strip coordinate detectors. Plane angle α_{x2}^{strip} is the estimation of the electron trajectory deviation after the multiple Coulomb scattering in first, second, and third tungsten layers. It is calculated using the information from second and

third planes of silicon strip coordinate detectors. Plane angle α_{x2} is the estimation of the electron trajectory deviation after the multiple Coulomb scattering in third tungsten layer. It is calculated subtracting electron trajectory deviation in first and second tungsten layers: $\alpha_{x2} = \alpha_{x2}^{strip} - \alpha_{x1}$. Plane angles α_{y1} and α_{y2} are calculated in the same manner.

Fig. 5a and b show the couple of distributions for plane angles α_{x1} , α_{y1} and α_{x2} , α_{y2} resulting from vertical electron beam with energy of 10 MeV, respectively. All these distributions are very similar and have approximately the same shape and width. Fig. 5c shows the total distribution including for each event the values: α_{x1} , α_{y1} , α_{x2} , and α_{y2} . Combining the Gaussians of these angles into one quantity assumes that there is negligible energy lost in each tracker-converter layer, thus causing the scattered angle distribution to be similar. The distributions in Fig. 5 are centered at 0^0 angle, as each elementary act of scattering has equal probability for any direction. Each distribution can be approximated by Gaussian due to the Central Limit Theorem, because each elementary act of scattering is statistically independent. Mean squared angle of multiple scattering has dependence $1/E$, which is the main point for the next analysis. The Gaussian approximation for total distribution has the standard deviation:

$$\sigma = 12.70^0 \pm 0.07^0$$

The dependence of standard deviation for the Gauss approximation of total distribution (like shown in Fig. 5c) from the energy of electron is shown in Fig. 6. There are two lines: first one is for vertical beam (black line) and another one is for initial beam inclination of 30^0 (red line). The value of the standard deviation estimated for 10 MeV is also marked.

The curve from Fig. 6 is used to evaluate the energies of electron (E^-) and positron (E^+) using the estimation of standard deviation for the values α_{x1} , α_{y1} , α_{x2} , α_{y2} for each component of the pair:

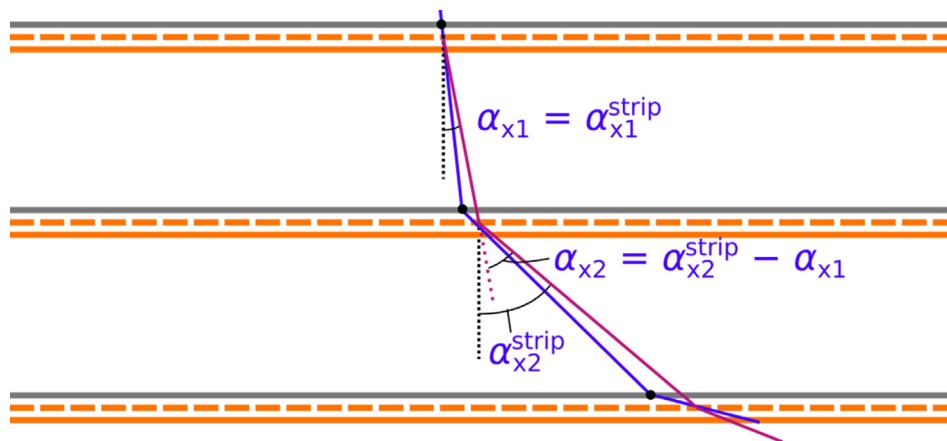


Fig. 4. An example of electron trajectory in the GAMMA-400 converter-tracker (blue line). The trajectory of electron restored using information from silicon strip detectors (magenta line). The estimation of the electron trajectory deviation after the multiple Coulomb scattering in first and second tungsten layers (α_{x1}). The estimation of the electron trajectory deviation after the multiple Coulomb scattering in third tungsten layer (α_{x2}). (For interpretation of the references to colour in this figure legend, the reader is referred to the web version of this article.)

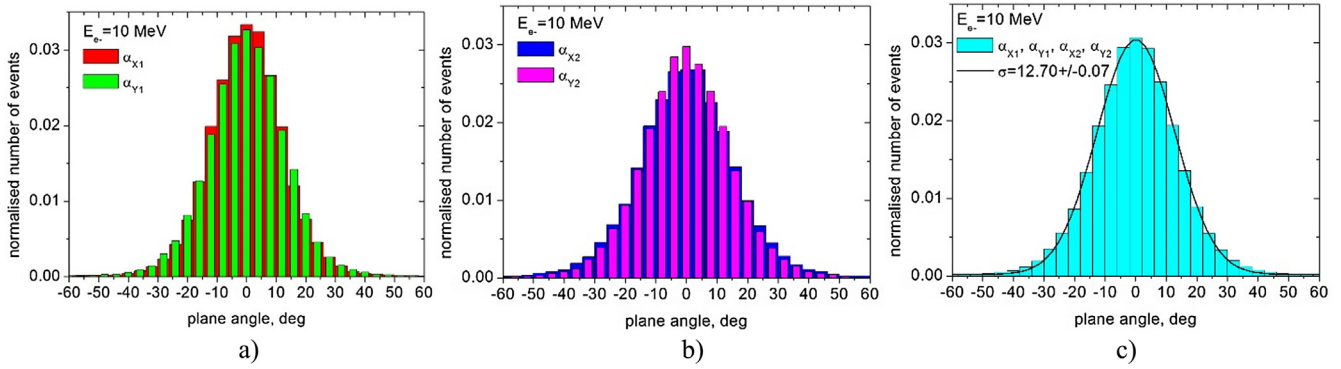


Fig. 5. The couple of distributions for plane angles α_{x1} , α_{y1} (a) and α_{x2} , α_{y2} (b). The total distribution including for each event the values: α_{x1} , α_{y1} , α_{x2} , α_{y2} (c).

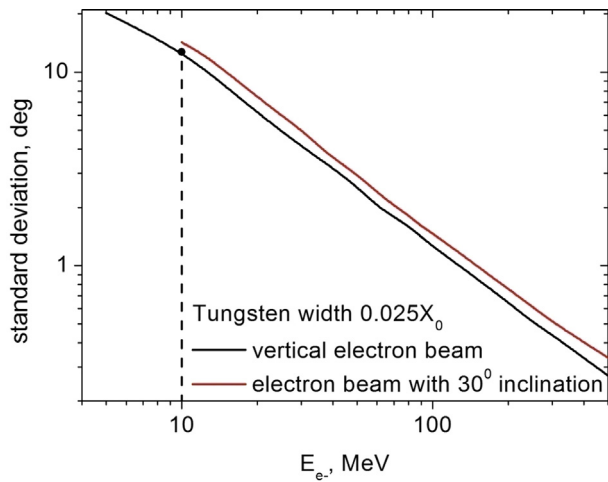


Fig. 6. The dependence of standard deviation for Gauss approximation of total distribution (Fig. 5c) from the energy of electron beam. Black line corresponds to the vertical beam, red line to the beam with inclination 30° . The value of the standard deviation estimated for 10 MeV is marked by black point. (For interpretation of the references to colour in this figure legend, the reader is referred to the web version of this article.)

$$\langle \sqrt{\theta^2} \rangle = \sqrt{\frac{(\alpha_{x1} - \bar{\alpha})^2 + (\alpha_{y1} - \bar{\alpha})^2 + (\alpha_{x2} - \bar{\alpha})^2 + (\alpha_{y2} - \bar{\alpha})^2}{4}}, \quad (3)$$

$$\text{where } \bar{\alpha} = \frac{\alpha_{x1} + \alpha_{y1} + \alpha_{x2} + \alpha_{y2}}{4}.$$

Such energy estimation should be considered only as procedure to evaluate relative energy contributions in (1), (2). The initial energy of pair components is not the same, therefore, it is possible for some electron/positron having low energy (< 5 MeV). For this low-energy range the linear extrapolation procedure is used applying the data for higher energy. The restored energy distribution for some initial energy of electron beam has long arm high-energy tail, but the average value of the distribution is well estimated. Fig. 7a shows the calibration dependence of the average value of restored energy for vertical electron beam. It is evident that this dependence is practically linear. The energy resolution, estimated as 68% containment, for the restored energies is shown in Fig. 7b. It is approximately constant in the considered energy range up to 150 MeV.

Considered methods allow us to calculate the plane angles α_x and α_y of initial gamma from plane angles of e^+/e^- pair, using (1) and (2). In the spherical coordinate system, zenith and polar angles (θ and φ) of initial gamma are calculated from the following relations:

$$\tan^2(\theta) = \tan^2(\alpha_x) + \tan^2(\alpha_y), \quad (4)$$

$$\tan(\varphi) = \frac{\tan(\alpha_x)}{\tan(\alpha_y)}. \quad (5)$$

The angle δ of deviation of reconstructed direction (θ , φ) from true direction (θ_0 , φ_0) of initial gamma is calculated as:

$$\delta = \arccos\left(\frac{\sin\theta \times \cos\varphi \times \sin\theta_0 \times \cos\varphi_0 + \sin\theta \times \sin\varphi \times \sin\theta_0 \times \sin\varphi_0}{\cos\theta_0 \times \cos\theta}\right). \quad (6)$$

Fig. 8 shows four distributions of deviation angles for initial gamma-ray energies 20, 50, 100, and 150 MeV are shown. Angular resolution is determined as a location of vertical line on the distribution contained 68% of events from the left side. Such estimation is marked as $\text{psf}_{68\%}$.

The energy dependence of the GAMMA-400 angular resolution for thin layers of tungsten calculated with proposed methods is shown in Fig. 9 by red line. The results of previous calculations from (Leonov et al., 2017) are also shown using green line. Improved energy weights estimation in (1), (2) allows us to have $\sim 25\%$ better angular resolution. The theoretical limitation for GAMMA-400, based on multiple scattering in couple of thin tungsten layers, is shown in Fig. 9 by blue dashed line. This limitation was calculated using the following relation (Highland, 1975; Lynch and Dahl, 1991):

$$\theta = \frac{13.6 \text{ MeV}}{\beta c p} z \sqrt{\frac{X}{X_0}} \times \left[1 + 0.038 \times \ln \frac{X}{X_0} \right], \quad (7)$$

where z is particle charge, β is particle velocity, pc is particle energy in MeV, X_0 is radiation length of the matter, X is thickness of the matter.

As the efficiency and quality of track reconstruction is not considered in the calculations, the comparison with angular resolution (68% containment) of Fermi-LAT

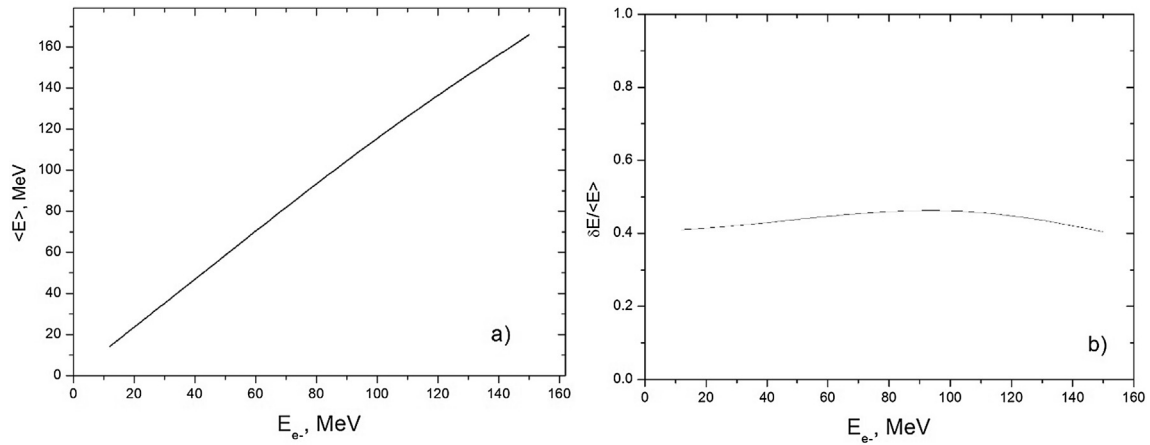


Fig. 7. The calibration dependence of the average value of restored energy for vertical electron beam (a). The energy resolution was estimated as 68% containment (b).

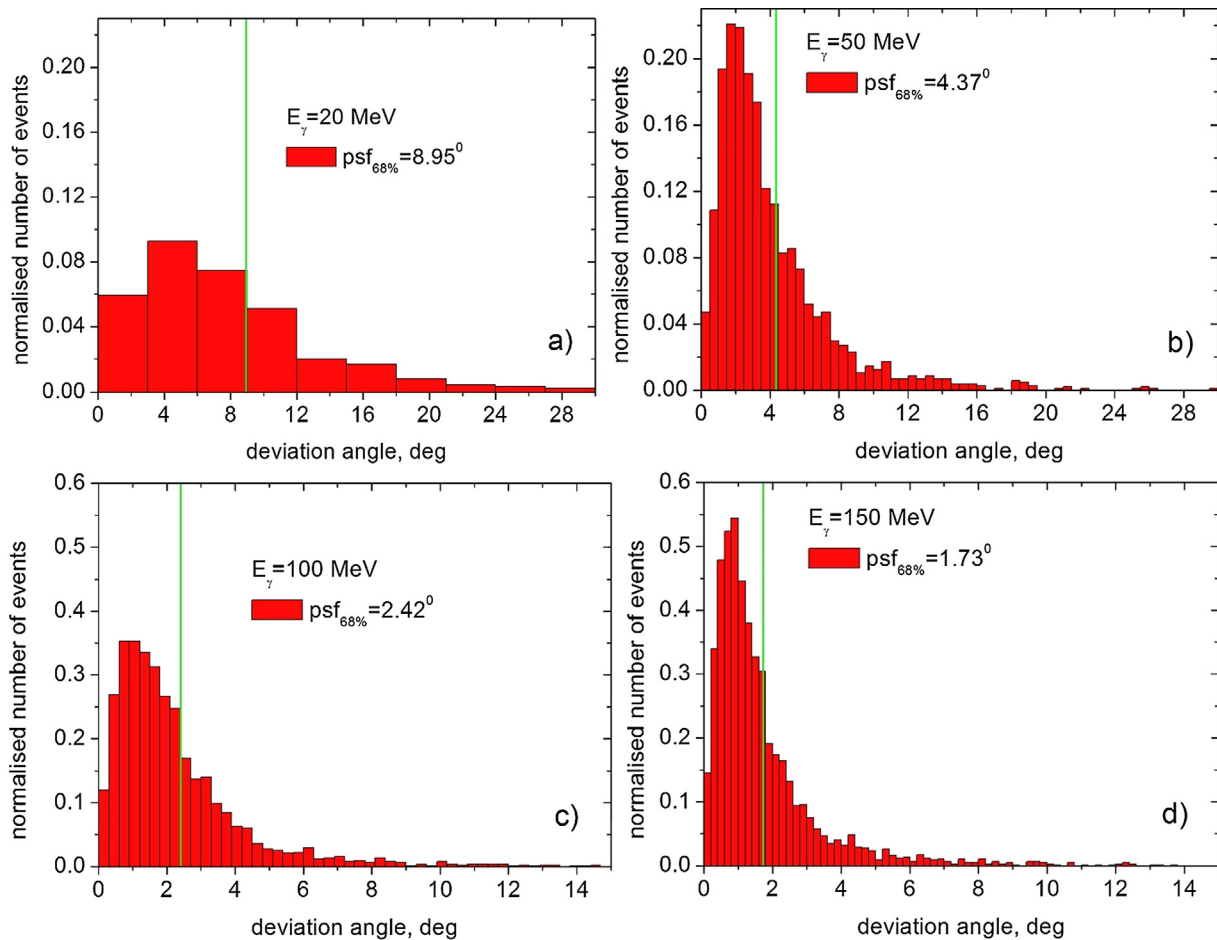


Fig. 8. The distributions of deviation angles for initial gamma-ray energies 20 (a), 50 (b), 100 (c), and 150 MeV (d).

(http://www.slac.stanford.edu/exp/glast/groups/canda/lat_Performance.htm) in front configuration with thin tungsten layers is also shown in Fig. 9. In energy range from 20 to

50 MeV, the estimated angular resolution of GAMMA-400 is 40% better than angular resolution of Fermi-LAT in configuration with thin tungsten foils.

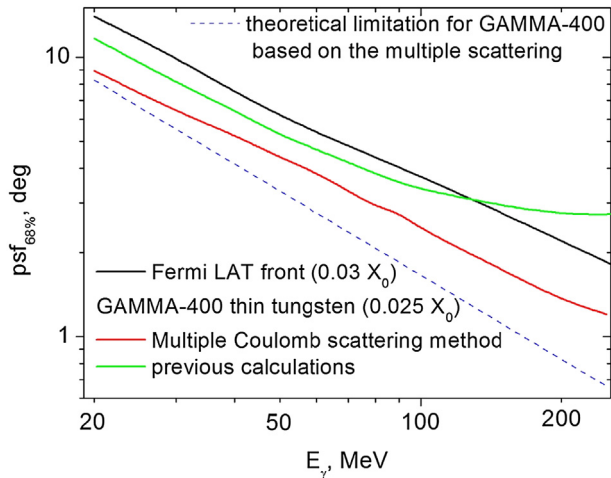


Fig. 9. The energy dependence of GAMMA-400 angular resolution for thin layers of tungsten in converter-tracker is presented by red line. The results of previous calculations from (Leonov et al., 2017) are also shown by green line. The theoretical limitation for GAMMA-400, based on multiple scattering in couple of thin tungsten layers, is shown by blue dashed line. The angular resolution of Fermi-LAT in front configuration with thin tungsten layers is shown by black line. (For interpretation of the references to colour in this figure legend, the reader is referred to the web version of this article.)

5. Conclusions

The method to improve the reconstruction accuracy of incident angle for low-energy gamma rays in the GAMMA-400 space-based gamma-ray telescope is presented. Applying the energy dependence of multiple Coulomb scattering for pair components generated in converter-tracker, it is possible to estimate the energies for each particle, and to use those energies as weight in angle reconstruction procedure. To identify the unique track in different projections imaginary curvature method is applied. Such approach is the further development of the procedure proposed in (Kheymits et al., 2015) and (Leonov et al., 2017) and it allows us to have $\sim 25\%$ better angular resolution in the energy range from 20 to 150 MeV. Comparing presented results with the performance of Fermi-LAT in the configuration with thin tungsten foils, there is $\sim 40\%$ improvement for the energy range from 20 to 50 MeV.

Acknowledgements

This study was supported by the Russian State Space Corporation ROSCOSMOS (contract no. 024-5004/16/224).

References

- Acerro, F., Ackermann, M., Ajello, M., et al., 2015. Fermi large area telescope third source catalog. *Astrophys. J. Suppl. Ser.* 218 (2), 23, 1–41.
- Ackermann, M., Ajello, M., Allafort, A., et al., 2013. The first Fermi-LAT catalog of sources above 10 GeV. *Astrophys. J. Suppl. Ser.* 209, 1–34.
- Allison, J., Apostolakis, J., Lee, S.B., et al., 2016. Recent developments in Geant4. *Nucl. Instrum. Meth. A* 835, 186–225.
- Berra, A., Bonvicini, V., Lietti, D., et al., 2015. Study of the readout configuration of the GAMMA-400 silicon tracker sensors. *Nucl. Instrum. Meth. Phys. Res. A* 798, 80–87.
- De Angelis, A., Tatischeff, V., Grenier, I.A., et al., 2018. Science with e-ASTROGAM: a space mission for MeV-GeV gamma-ray astrophysics. *J. High Energy Astrophys.* 19, 1–106.
- Giuliani, A., Cocco, V., Mereghetti, S., et al., 2006. The AGILE on-board Kalman filter. *Nucl. Instrum. Meth. Phys. Res. A* 568, 692–699.
- Highland, V.L., 1975. Some practical remarks on multiple scattering. *Nucl. Instrum. Meth.* 129 (2), 497–499.
- Kheymits, M.D., Arkhangelskaja, I.V., Arkhangelskiy, A.I., et al., 2015. Method of incident low-energy gamma-ray direction reconstruction in GAMMA-400 gamma-ray space telescope. *Phys. Procedia* 74, 368–371.
- Leonov, A.A., Galper, A.M., Topchiev, N.P., et al., 2017. Modifications of a method for low energy gamma-ray incident angle reconstruction in the GAMMA-400 gamma-ray telescope. *IOP Conf. Ser.: Journal of Physics: Conf. Ser.* 798, 012012, 1–5.
- Lynch, G.R., Dahl, O.I., 1991. Approximations to multiple Coulomb scattering. *Nucl. Instrum. Meth., Section B* 58 (1), 6–10.
- Moiseev, A.A., Hartman, R.C., Ormes, J.F., et al., 2007. The anticoincidence detector for the GLAST large area telescope. *Astroparticle Phys.* 27, 339–358.
- Principe, G., Malyshev, D., Ballet, J., Funk, S., 2018. The first catalog of Fermi-LAT sources below 100. MeV. *Astron. Astrophys.* 618 (A22), 1–13.
- Schonfelder, V., Bennett, K., Blom, J.J., et al., 2000. The first COMTEL source catalogue. *Astron. Astrophys. Suppl. Ser.* 143, 145–179.
- Topchiev, N.P., Galper, A.M., Bonvicini, V., et al., 2016b. Perspectives of the GAMMA-400 space observatory for high-energy gamma rays and cosmic rays measurements. *IOP Conf. Ser.: J. Phys.: Conf. Series* 675, 032010.
- Topchiev, N.P., Galper, A.M., Bonvicini, V., et al., 2016a. The GAMMA-400 gamma-ray telescope for precision gamma-ray emission investigations. *IOP Conf. Ser.: J. Phys.: Conf. Ser.* 675, 032009.
- http://www.slac.stanford.edu/exp/glast/groups/canda/lat_Performance.htm (the data were accessed on May, 2018).